J Sol-Gel Sci Technol (2010) 55:135–141
DOI 10.1007/s10971-010-2225-6

Effect of nickel and cobalt ions on low temperature synthesis of mullite by sol–gel technique

Biswajoy Bagchi · Sukhen Das · Alakananda Bhattacharya · Ruma Basu · Papiya Nandy

Received: 26 March 2010 / Accepted: 16 April 2010 / Published online: 29 April 2010

Abstract Synthesis of mullite has been achieved at a low temperature of 600 °C by sol–gel technique in presence of nickel and cobalt ions. Samples were characterized by DTA, XRD, FESEM and FTIR spectroscopy. Mullite formation was found to depend on the concentration of the ions to a certain extent. Highly crystalline spherical mullite particles of dimension 35 nm were obtained at 0.02 M nickel or cobalt concentration.

Keywords Mullite · Sol–gel · Low temperature · XRD · Nickel · Cobalt

1 Introduction

Mullite, a highly stable ceramic has been of particular interest to several researchers because of its exceptionally high mechanical strength, chemical stability, low dielectric constant, high creep resistance and low thermal expansion co-efficient [1–8]. Conventionally, mullite formation starts above 1200 °C completing at around 1600 °C by solid state reaction between Al_2O_3 and SiO_2 particles [9–15]. However, it has been well documented by many that when mullite precursors are mixed at an atomic level the temperature of mullitization can be decreased to 1000 °C. Atomic level mixing of precursors is best achieved via sol–gel route by using a salt of aluminium and Tetraethylorthosilicate (TEOS) and is the most preferred way till date because of the chemical homogeneity of the precursors and high purity of the end product [16–21].

The low synthesis temperature can also be attained by adding certain mineralizers for example Kiss et al. showed that Cu^{2+}, Mn^{2+} and Fe^{3+} can induce accelerated phase transformations in alumina and kaolinite leading to mullite formation at low temperatures. Kong et al. used V_2O_5 to accelerate mullite phase formation in solid state reaction while B_2O_3 has been used by Hong et al. to the same effect in diphasic gels. Transition metal ions generally induce their effect by interacting with the silica layer and destabilizing the aluminium–silicate matrix [22–27].

However in all the cases the mullite formation does not occur below 1000 °C, also phase pure mullite is obtained only at higher temperatures. We, in this work report synthesis of phase pure nanocrystalline mullite via sol–gel route at 600 °C by using Ni^{2+} and Co^{2+} as mineralizing agents and also studied the effect of their concentration on the phase transformation of mullite precursor gel.

2 Experimental

Mullite precursor gel powder was synthesized by dissolving stoichiometric amounts of Al(-O-i-Pr)$_3$ (puriss, Spectrochem Pvt. Ltd., Mumbai, India) and TEOS (Merck, Honnenbrun, Germany) in 0.5 (M) solution of $Al(NO_3)_3 \cdot 9H_2O$ (extra pure, Merck, Worli, Mumbai, India). The

B. Bagchi · S. Das (✉) · P. Nandy
Physics Department, Jadavpur University,
Kolkata 700 032, India
e-mail: sukhendasju@rediffmail.com

B. Bagchi
e-mail: biswajoy_ju@rediffmail.com

A. Bhattacharya
Physics Department, West Bengal State University,
Barasat, India

R. Basu
Physics Department, Jogamaya Devi College,
Kolkata 700 026, India

Table 1 Sample designation

Sample	Composition
G0	ANN + Al(-OiPr$_3$)$_3$ + TEOS
N1	G0 + 0.02(M)Ni
N2	G0 + 0.1(M)Ni
N3	G0 + 0.5(M)Ni
C1	G0 + 0.02(M)Co
C2	G0 + 0.1(M)Co
C3	G0 + 0.5(M)Co

molar ratio of Al(-O-i-Pr)$_3$/Al(NO$_3$)$_3$·9H$_2$O was kept at 3.5 in order to form spinnable sols. The mole ratio of Al/Si was 3 and the pH of the solution was measured to be 5. After 3 h of vigorous stirring, the sol was maintained overnight at 60 °C. Gel formation took place after 24 h and was optically transparent. Finally, the gel was dried at 105 °C and ground to a free flowing powder [27, 28].

Metal doped gels were prepared by adding different concentrations of corresponding metal salt solution (NiCl$_2$·6H$_2$O and (CH$_3$COO)$_2$Co·4H$_2$O) to the initial mixture before stirring and same steps were followed as described above. The doped gel powders were colored green and purple for Ni^{2+} and Co^{2+} respectively. The composition and designation of the doped powder samples synthesized is tabulated below (Table 1). The powdered samples were then sintered at 600, 1000 and 1400 °C for 2 h.

Themal behavior of the gel samples were studied by a simultaneous DTA-TG (DTG-60H, Shimadzu (Asia Pacific) Pte. Ltd., Singapore) analyzer operating at the rate of 10 °C/min under N_2 flow. Crystalline phases were studied by X-ray diffractometer (Bruker AXS Inc., Madison, WI) with 2θ varying from 10 to 70 °C. Fourier Transform Infrared (FTIR-8400S, Shimadzu) spectroscopy was carried out to analyze the bending and stretching vibrations. The samples were pelletized after mixing 1% sample with spectroscopy grade KBr and then analyzed by FTIR using pure KBr pellet as background from 1200 to 400 cm^{-1}. Morphology of the sintered gels were observed by Field Emission Scanning Electron Microscope (FESEM) (JSM 6700F, JEOL Ltd. Tokyo, Japan).

3 Results & discussion

The DTA pattern shows basically two endothermic peaks below 400 °C corresponding to evolution of volatile components e.g. water, alcohol from the gel powder and a sharp exothermic peak for its transformation into mullite (Fig. 1). The native gel (without nickel or cobalt) gave the exothermic peak at 999.2 °C but upon addition of nickel

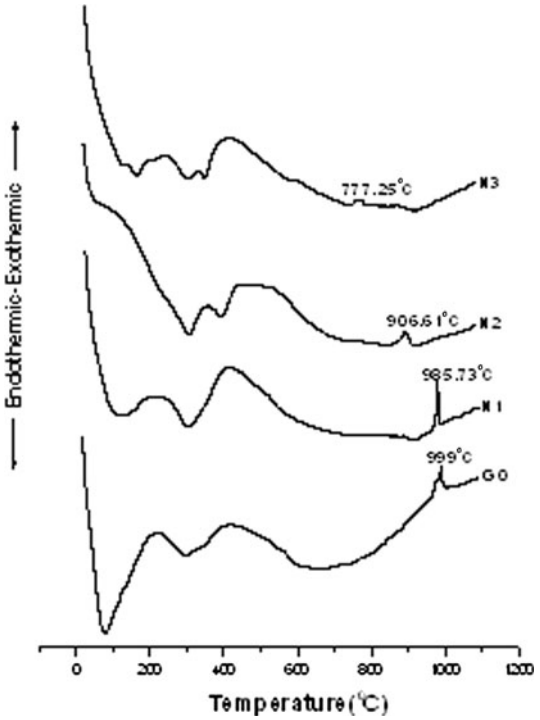

Fig. 1 DTA pattern of nickel doped gels

ions a sharp exothermic peak was obtained which is shifted to lower temperature by 10 °C. The position of this peak further continued to shift on increasing the concentration of nickel. At 0.5 M Ni^{2+} concentration the gel transformed with a much diffused peak at around 777.25 °C (Fig. 1 N3). For cobalt doped samples, the shift of the exothermic peak was small compared to nickel doped samples and sample C3 gives a single sharp exothermic peak at 302 °C which corresponds to the formation of CoO phase [29–31] (Fig. 2). This was further supported by the intense blue coloration of the sintered sample.

The sintered gel samples were analyzed by X-ray diffraction operating at 40 kV with a scan speed of 0.5 step/sec. The raw scan data was refined by Rietveld technique whereby preferred orientation, absorption contrast, intensity aberrations and amorphous material content were taken into account. Figure 3 shows sharp characteristic peaks of mullite in the Ni^{2+} doped samples at 600 °C compared to the native gel sample. However with increasing nickel concentration the intensity of the peaks decrease and ultimately no mullite phase was detected in sample N3.

In case of cobalt doped sintered gels (Fig. 4), appreciable mullite phase was detected only in case of sample C1 in which the concentration of cobalt was lowest. Also the amount of mullite phase was greater in N1 than C1 as can be seen from both DTA and XRD pattern. This suggests that Ni^{2+} interacts with the aluminium silicate matrix to a greater extent than cobalt which may be attributed to the difference in complex forming ability of the two ions

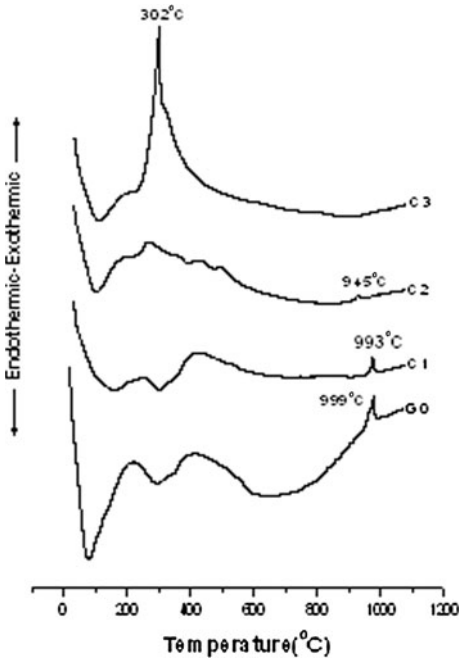

Fig. 2 DTA pattern of cobalt doped gels

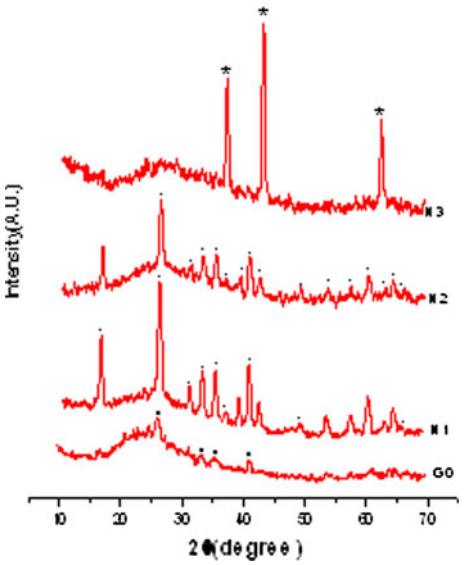

Fig. 3 XRD pattern of nickel doped gels sintered at 600 °C for 2 h. *Marks* indicate assignment of peaks: (●) Mullite, (*) Nickel Oxide

with the gel matrix. Thus at low concentration both cobalt and nickel ions can effectively induce accelerated transformation of the gels into mullite but after reaching a critical concentration the gel cannot transform to mullite at 600 °C. In fact, at 0.5 M concentration (and at 600 °C), nickel doped gels transforms to crystalline nickel oxide phase rather than mullite whereas cobalt doped gels gives cobalt oxide [31, 32]. At high enough doping concentration

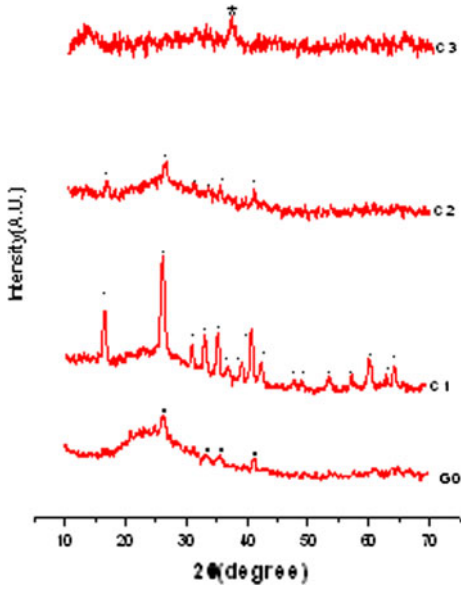

Fig. 4 XRD pattern of cobalt doped gels sintered at 600 °C for 2 h. *Marks* indicate assignment of peaks: (●) Mullite, (*) Nickel Oxide

the initial gel formation was inhomogeneous due to excess metal ions and reaction primarily drives in the direction of their corresponding oxide formation (Fig. 3 N3 and Fig. 4 C3).

Although, DTA pattern shows the exothermic peak around 980 °C but actually mullite formation starts at much lower temperature of 600 °C. This is due to the fact that DTA analysis being a dynamic process can't detect the nanocrystalline mullite phase which is present at this low temperature [27].

Such accelerated transformation was achieved due to complex forming ability of the transition metal ions in the alumino-silicate matrix [21, 23]. It has been shown in case of copper doped sol–gel derived mullite that due to Jahn–Teller effect a strain develops in the matrix which ultimately leads to the low temperature phase transformation of precursor gel into mullite. Also such low temperature transformation will consequently lead to nanocrystalline phase [27].

The observed difference in mullite formation from cobalt and nickel may be similarly explained as follows. In a moderately weak ligand field (here oxide) both Ni^{2+} and Co^{2+} will be in high spin configuration. The unpaired electron in the t_{2g} orbital of Co^{2+} (d^7) will cause Jahn–Teller distortion of CoO_6 octahedra in the gel matrix which may account for the accelerated transformation. In case of Ni^{2+} there will be no distortion due to symmetrically filled e_g and t_{2g} orbital but the comparatively small ionic radius of high spin nickel cation may effectively increase metal–ligand interaction resulting in development of strain throughout the matrix and hence inducing low temperature

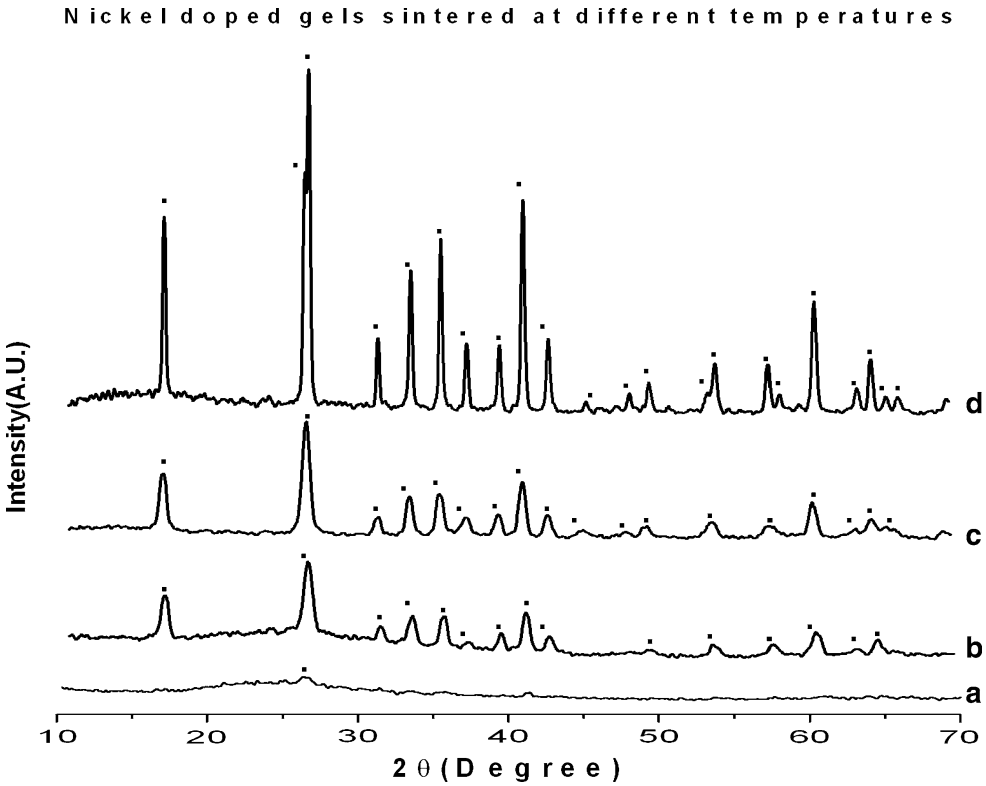

Fig. 5 XRD pattern of N1gel sintered at different temperatures for 2 h. (*a*) G0 at 600 °C, (*b*) N1 at 600 °C, (*c*) 1000 °C, and (*d*) 1400 °C for 2 h. *Marks* indicate assignment of peaks: (●) Mullite

phase transformation of the gel. The proposed strain developed in the matrix will be less in case of Co^{2+} because contribution from Jahn–Teller distortion due to Co^{2+} will be very small as t_{2g} orbital do not lie directly in the path of the ligand in an octahedral field [33, 34]. It can be seen from Figs. 3 & 4 that at 0.02 M and 0.1 M concentration, Ni^{2+} doped gels gives much pronounced characteristic mullite peaks than Co^{2+}.

Figure 5 shows crystal phase development in N1 sintered at three different temperatures. The extent of mullitization is almost same in case of 600 and 1000 °C sintered samples which indicate the role of nickel in accelerating the phase transformation. The sharp peaks at 1400 °C are due to complete mullitization expected at such high temperature. Similar argument can be made for C1 (Fig. 6) where cobalt doped sintered gels shows increased mullite content with temperature. However it is to be noted that the native gel remained amorphous at 600 °C.

The morphology of the mullite particles were investigated by FESEM with samples N1 and C1 (both sintered at 600 °C for 2 h). The micrograph for N1 shows almost round shaped particles of mullite of average size 30–45 nm. The large irregular particles seen in the micrograph are aggregations of small mullite particles [27, 35] (Fig. 7).

Sample C1 shows more distinct spherical morphology of mullite particles of size 30 nm embedded in the matrix. Numerous smaller particles can also be seen along with some amorphous aggregates (Fig. 8). The mullite content in sample N1 is much greater than C1 as can be seen from the more dense packing of the mullite particles. The size of the mullite particles conforms well with the size calculated from the X-ray diffraction data (not shown) using Debye-Sherrer formula.

The characteristic stretching and bending modes of vibration of chemical bonds of a sample can be effectively evaluated by FTIR spectroscopy. Pure mullite samples (prepared using KBr pellet method) gives characteristic bands at wave numbers around 560, 730, 840, 1060, 1130 and 1170 cm^{-1} [36–39].

Figure 9 shows the FTIR spectra of the nickel doped sintered gels. All the characteristic bands of mullite-564(alumina octahedra), 730(alumina tetrahedra), 838(alumina tetrahedra) and 1126 cm^{-1} (Si–O stretching mode) appear in samples N1 and N2 but in the latter the bands are less prominent. N3 do not show any appreciable bands, however, it has a prominent band at around 450 cm^{-1} which may be due to Ni–O bond in nickel oxide phase.

Similarly, cobalt doped sintered gels also produce the mullite characteristic bands except C3 which gives two bands one around 570 and another at 680 cm^{-1} which are characteristic vibration mode bands of Co–O bond [31, 40]. The bands obtained are weak compared to nickel doped gels at same concentration (Fig. 10).

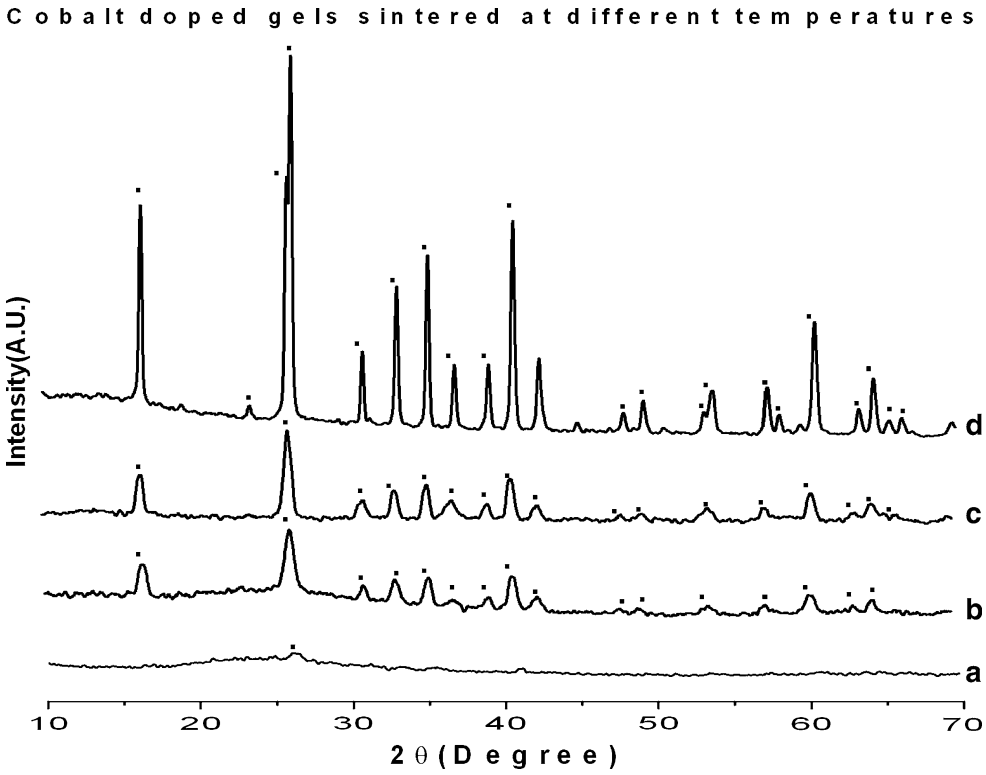

Fig. 6 XRD pattern of C1gel sintered at different temperatures for 2 h. (*a*) G0 at 600 °C, (*b*) C1 at 600 °C (*c*) 1000 °C (*d*) 1400 °C for 2 h. *Marks* indicate assignment of peaks: (●) Mullite

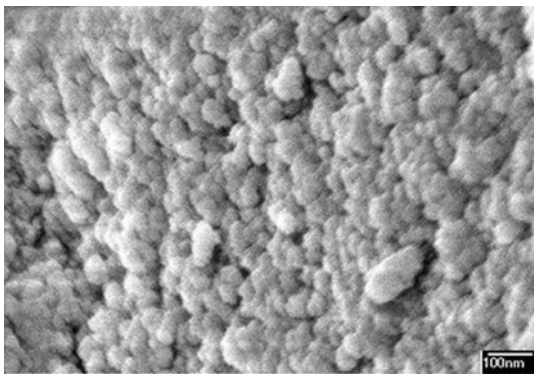

Fig. 7 FESEM micrograph of N1 sinterd at 600 °C

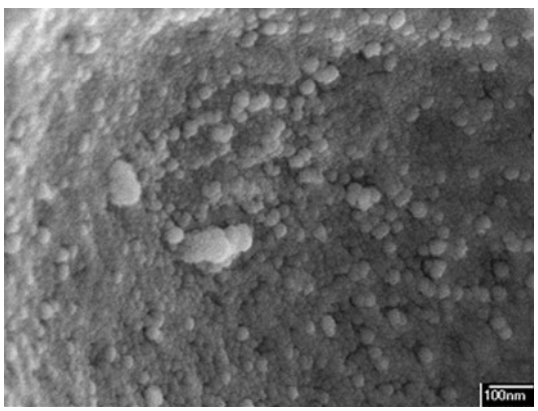

Fig. 8 FESEM micrograph of C1 sinterd at 600 °C

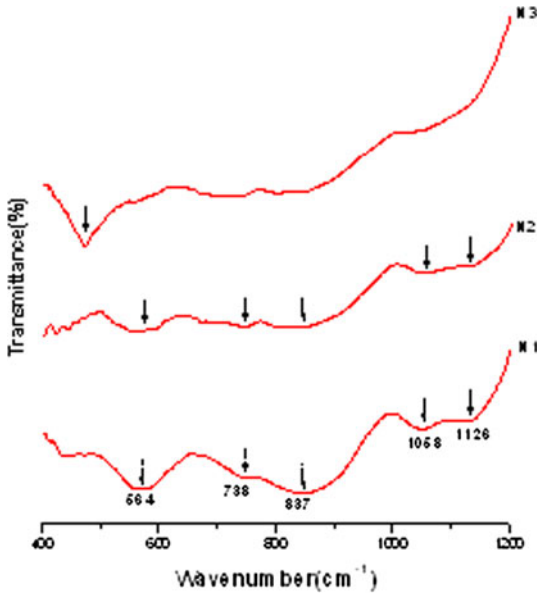

Fig. 9 FTIR spectra of nickel doped gels sintered at 600 °C for 2 h

4 Conclusion

Accelerated phase transformation of mullite precursor gel has been achieved via sol–gel method by co-doping with nickel and cobalt ions at 600 °C. A comparative study has been performed relating to the dependence of mullite formation on the metal ion concentration. The result shows that maximum mullite phase is detected in the sintered gels

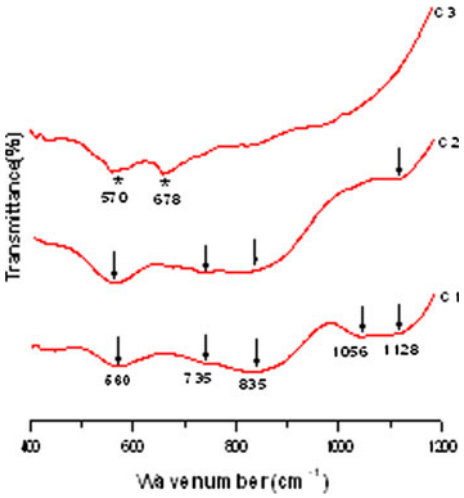

Fig. 10 FTIR spectra of cobalt doped gels sintered at 600 °C for 2 h

at 600 °C and at 0.02 M concentration for both ions. The size of the mullite particle is within 40 nm approximately. With increase in concentration of the doping ion, extent of mullite formation decreases and is inhibited at 0.5 M. Nickel ion induces formation of mullite phase to a higher extent than cobalt. The low temperature formation of mullite phase and the higher reactivity of Ni^{2+} may be explained by the increased metal–ligand interaction due to small high spin Ni^{2+} in the gel matrix. The weak Jahn–Teller distortion by Co^{2+} due to unsymmetrical filling of t_{2g} orbital and comparatively large ionic radius (and hence consequent weak metal–ligand interaction) is effective in inducing accelerated transformation but to a lower extent than nickel.

Acknowledgments We are grateful to DST, Government of India, for financial assistance.

References

1. Perera DS, Allott G (1985) Mullite morphology in fired kaolinite/hallosite clays. J Mater Sci Lett 4:1270–1272
2. Vol'khin VV, Kazakova IL, Pongratz P, Halwax E (2000) Mullite Formation from Highly Homogeneous Mixtures of Al_2O_3 and SiO_2. Inorg Mater 36(4):375–379
3. Schneider H, Schreuer J, Hildmann B (2008) Structure and properties of mullite-a review. J Eur Ceram Soc 28(4):329–344
4. Schmücker M, Schneider H (2005) Mullite-type gels and glasses. In: Schneider H, Komarneni S (eds) Mullite. Wiley-VCH, Weinheim
5. Rahman S, Freimann S (2005) The real structure of mullite. In: Schneider H, Komarneni S (eds) Mullite. Wiley-VCH, Weinheim
6. Schreuer J, Hildmann B, Schneider H (2006) Elastic properties of mullite single crystals up to 1400 °C. J Am Ceram Soc 89:1624–1631
7. Davis RF, Pask JA, Somiya S (1990) Mullite and mullite matrix composites ceramic transactions. American Ceramic Society, Westerville
8. Aksay IA, Dabbs DM, Sarikaya M (1991) Mullite for structural, electronic and optical applications. J Am Ceram Soc 74(10):2343–2354
9. Sahnoune F, Chegaar M, Saheb N, Goeuriot P, Valdivieso F (2008) Algeria kaolinite used for mullite formation. Appl Clay Sci 38:304–310
10. Chen Y-F, Wang MC, Hon MH (2004) Phase transformation and growth of mullite in kaolin ceramics. J Eur Ceram Soc 24:2389–2397
11. Viswabaskarana V, Gnanama FD, Balasubramanian M (2004) Mullite from clay-reactive alumina for insulating substrate application. Appl Clay Sci 25:29–35
12. Pascual J, Zapatero J (2000) Preparation of mullite ceramics from coprecipitated aluminium hydroxide and kaolinite using hexamethylenediamine. J Am Ceram Soc 83(11):2677–2680
13. Viswabaskarana V, Gnanama FD, Balasubramanian M (2003) Mullitisation behavior of calcined clay-alumina mixtures. Ceram Int 29:561–571
14. Tang YF, Ling ZD, Lu YN, Li AD, Ling HQ, Wang YJ, Shao QY (2002) Study on the densification of composite coating particles of α-Al_2O_3-SiO_2. Mater Chem Phys 75:265–269
15. Viswabaskarana V, Gnanama FD, Balasubramanian M (2002) Ceram Int 28:557–564
16. Cassidy DJ, Woolfrey JL, Bartlett JR, Ben-Nissan B (1997) The effect of precursor chemistry on the crystallization and densification of sol–gel derived mullite gels and powders. J Sol–Gel Sci Technol 10:19–30
17. Komarneni S, Rutiser C (1996) Single-phase and diphasic aerogels and xerogels of mullite: preparation and characterization. J Eur Ceram Soc 16:143–147
18. Campos AL, Silva NT, Melo FCL, Oliveira MAS, Thim GP (2002) Crystallization kinetics of orthorhombic mullite from diphasic gels. J Non-Cryst Solids 304:19–24
19. Marques Fonseca AML, Ferreira JME, Miranda Salvado IM, Baptista JL (1997) Mullite based compositions prepared by sol–gel techniques. J Sol–Gel Sci Technol 8:403–407
20. Huang YX, Senos AMR, Rocha J, Baptista JL (1997) Gel formation in mullite precursors obtained via tetra ethyl orthosilicate (TEOS) pre-hydrolysis. J Mater Sci 32:105–110
21. Mizukami F, Maeda K, Toba M, Sano T, Niwa SI (1997) Effect of organic ligand used in sol-gel process on the formation of mullite. J Sol Gel Sci Technol 8:101–106
22. Kiss EE, Putanov PS (2002) Influence of transition metal ions on the textural properties of alumina and aluminosilicate. React Kinet Catal Lett 75(1):39–45
23. Ferreira da Silva MG (1998) Role of MnO on the mullitization behaviour of Al_2O_3-SiO_2 gels. J Sol–Gel Sci Technol 13:987–990
24. Kong LB, Gan YB, Ma J, Zhang TS, Boey F, Zhang RF (2003) Mullite phase formation and reaction sequences with the presence of pentoxides. J Alloys Compd 351:264–272
25. Martigius T, Giraitis R (2002) Influence of copper oxide on mullite formation from kaolinite. J Mater Chem 13:121–124
26. Hong SH, Cermignani W, Messing GL (1996) Anisotropic grain growth in seeded and B_2O_3-doped diphasic mullite gels. J Eur Ceram Soc 16(18):133–141
27. Bagchi B, Das S, Bhattacharya A, Basu R, Nandy P (2009) Nanocrystalline mullite synthesis at a low temperature: effect of copper ions. J Am Ceram Soc 92(3):748–751
28. Song KC (1998) Preparation of mullite fibers from aluminium isoprpoxide-aluminium nitrate-tetraethylorthosilicate solutions by sol-gel method. Mater Lett 35(5–6):290–296
29. Mohamed MA, Halawy SA, Ebrahim MM (1994) The non-isothermal decomposition of cobalt acetate tetrahydrate. A kinetic and thermodynamic study. J Therm Ana 41:387–404

30. Wanjun T, Donghua C (2007) Mechanism of thermal decomposition of cobalt acetate tetrahydrate institute of chemistry, Slovak Acad Sci. doi: 10.2478/s11696-007-0042-3
31. Dharmaraj N, Prabu P, Nagarajan S, Kim CH, Park JH, Kim HY (2006) Synthesis of nickel oxide nanoparticles using nickel acetate and Poly(vinyl acetate) precursor. Mater Sci Eng B 128: 111–114
32. Glaspell GP, Jagodzinski PW, Manivannan A (2004) Formation of cobalt nitrate hydrate, cobalt oxide and cobalt nanoparticles using laser vaporization controlled condensation. J Phys Chem B 108:9604–9607
33. Burns RG (1993) Mineralogical applications of crystal field theory. Cambridge University Press, Great Britain
34. Stucki JW (1979) Advanced chemical methods for soil and clay minerals research. D. Reidel Publishing Company, Holland
35. Baranwal R, Villar MP, Garcia R, Laine RM (2001) Flame spray pyrolysis of precursors as a route to nanomullite powder: powder characterization and sintering behaviour. J Am Ceram Soc 84:951–961
36. Petit S (2006) In: Bergaya F, Theng BKG, Lagaly G (eds) Handbook of clay science, Developments in clay science. Elsevier, Amsterdam
37. Ore'fice RL, Vasconselos WL (1997) Sol-Gel transition and structural evolution on multicomponent gels derived from alumina silica system. J Sol–Gel Sci Technol 9:239–249
38. Beran A, Voll D, Schneider H (2001) Dehydration and structural development mullite precursors: an FTIR spectroscopic study. J Eur Ceram Soc 21:2479–2485
39. Shoval S, Boudeulle M, Yariv S, Lapides I, Panczer G (2001) Micro-raman and FT-IR spectroscopy study of thermal transformation of St. Claire Dickite. Opt Mater 16:319–327
40. Ortega-Zarzosa G, Araujo-Andrade C, Compea′n-Jasso ME, Marti′nez JR (2002) Cobalt oxide/silica xerogels powders: X-ray diffraction, infrared and visible absorbtion studies. J Sol–Gel Sci Technol 24:23–29